Printable Electrolytes: Tuning 3D-Printing by Multiple Hydrogen Bonds and Added Inorganic Lithium-Salts

Harald Rupp, Rajesh Bhandary, Amit Kulkarni, and Wolfgang Binder*

Here, the 3D-printing of supramolecular polymer electrolytes is reported, able to be manufactured via 3D-printing processes, additionally dynamically compensating for volume changes. A careful mechanical design, in addition to rheological effects observed for different additives to the electrolyte, is investigated and adjusted, in order to achieve printability via an extrusion process to generate a conductive electrode material. Qudruple-hydrogen bonds (UPy) act as supramolecular entities for the desired dynamic properties to adjust printability, in addition to added LiTFSi-salts to achieve ionic conductivities of $\approx 10^{-4}$ S cm^{-1} at T = 80 °C. Three different telechelic UPy-PEO/PPO-UPy-polymers with molecular weights ranging from Mn = 600–1500 g mol^{-1} were investigated in view of their 3D-printability by FDM-processes. It is found that there are three effects counterbalancing the rheological properties of the polymers: besides temperatures, which can be used as a known tool to adjust melt-rheology, also the addition of lithium-salts in junction with the polymers crystallinity exerts a major toolbox to 3D-print these electrolytes. Using specific compositions with Li/EO-ratios from 20:1, 10:1, and 5:1, the rheological profile can be adjusted to reach the required printability window. AT-IR-investigations clearly indicate a weakening of the UPy-bonds by the added Li$^+$ ions, in addition to a reduction of the crystallinity of the PEO-units, further changing the rheological profile. The so generated electrolytes are printable systems for novel electrolytes.

1. Introduction

An important desire in modern energy-technology is the generation of safer energy storage devices, able to meet modern consumer needs. Among those quests is the ability of an electrode/electrolyte material to compensate for damages imparted

H. Rupp, R. Bhandary, A. Kulkarni, W. Binder
Macromolecular Chemistry
Division of Technical and Macromolecular Chemistry
Institute of Chemistry
Faculty of Natural Sciences II (Chemistry, Physics and Mathematics)
Martin Luther University Halle-Wittenberg
von-Danckelmann-Platz 4, D-06120 Halle, Germany
E-mail: wolfgang.binder@chemie.uni-halle.de

The ORCID identification number(s) for the author(s) of this article can be found under https://doi.org/10.1002/admt.202200088.

during charging/discharging cycles, immanent in many energy-storage systems[1]. Thus, e.g., in the case of silicon electrodes,[2] large volume expansions generate cracks along the silicon-electrodes, in turn reducing their lifetimes significantly. There are a plethora of polymers able to repair and recover functionalities, primarily due to internal mechanical effects such as volume expansion or cracking, as well as via temperature-induced damage and decay, also including chemical degradation. Thus the development of devices displaying reversible functionalities, such as self-healing is particularly desirable for energy storage devices[3], since the lifetimes of many rechargeable batteries are limited due to the appearance of mechanical damage processes over the cycling processes[4]. One approach toward compensation of the rapid capacity fading due to the loss of electrical contact is the application of reversible, dynamic bonds[5], able to respond to internal or external changes, thus compensating for the volume-change associated with the charging/discharging cycle. As an example, the application of ureidopyrimidone (UPy) functionalized polymers[6], such as polyethylene glycol (PEG) (UPy-PEG-UPy) as a hydrogen-bonding self-healing binder led to excellent results[6b], achieving initial coulombic efficiencies (ICE) as high as 81% and a reversible capacity of 1454 mA h g^{-1} after 400 cycles corresponding to an average capacity decay of 0.04% per cycle. Deng and co-worker presented a quadrupole-bonded supramolecular polymer that can serve as self-healable binder for high-performance silicon nanoparticle (SiNP) anodes, by integrating a small amount of UPy moieties with a linear polymer poly(acrylic acid) (PAA).[6a] This supramolecular polymer offers strong adhesion strength with SiNP, which can withstand large volume expansion and release the internal stress of SiNP during the repeated lithiation/delithiation processes.
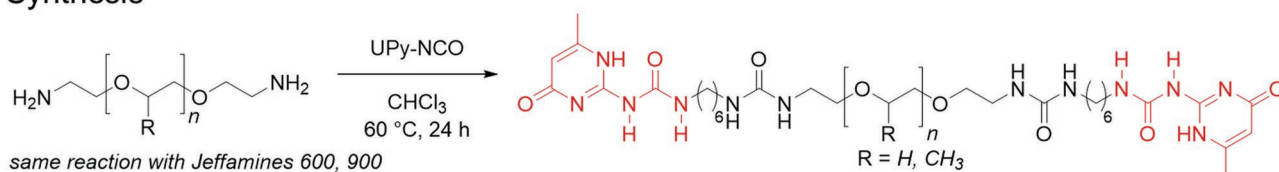
We here report the 3D-printing of a novel supramolecular polymer, able to be manufactured via 3D-printing processes, additionally including the ability to dynamically compensate for volume changes as reported earlier (**Figure 1**). A careful mechanical design, in addition to rheological effects observed for different additives to the electrolyte, is investigated and adjusted, in order to achieve printability via an extrusion process to generate a conductive electrode material. The manufacturing of electrodes via printing processes is important, as it would allow an easier fabrication process of
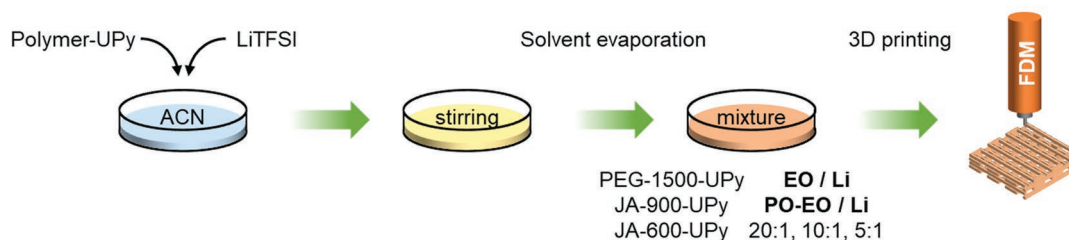
Figure 1. Chemical structure, synthesis, and 3D printing of telechelic, bivalent (2-ureido-4-pyrimidinone) PEG (PEG-1500-UPy), and telechelic, bivalent (2-ureido-4-pyrimidinone) Jeffamine (JA-x00-UPy). Electrolyte mixtures were prepared with LiTFSI for FDM (3D-printing).

many electrolyte systems. In traditional manufacturing of lithium-ion batteries, the polymer electrolyte is applied to the battery in a 2D planar process. For new and more complex electrolyte structures additive manufacturing, fused deposition modeling (FDM) can be used for 3D structures.[7] Such structures result in better electrochemical activity due to 3D diffusion of lithium ions, together with improvements on power, specific capacity.[8] When combining electrolyte 3D-printing directly with 3D-printing of electrodes dead-volume is excluded and the energy storage density can be maximized.[9] Early FDM-based electrolytes were based on PLA filaments or carbonate/LiClO$_4$ composites.[8b,9a,10] For lithium-based electrolytes often PEG was used due to its solvating properties for lithium ions, where the EO-oxygens interact with lithium ions influencing thermal and conducting properties toward good electrolytes.[11] At room temperature the materials suffer from a quite low conductivity (10^{-6}–10^{-8} S cm^{-1}), additionally displaying brittleness, thus cracking easily and harming the stability inside the battery.[12] With the addition of hydrogen bonding groups to the PEG polymer features of self-healing and/or shape-memory are embedded to suppress the formation of cracks. Thus even small cracks can be autonomously repaired based on intrinsic hydrogen bonds interactions, able to reversibly open and close after damage. Especially the use of ureidopyrimidine-quadruple bonds (UPy)[13] has become important, as these bonds open/close at only elevated temperatures, thus leading to quite strong and stiff materials at ambient temperatures. When applied to polymer electrolytes they lead to flexible and self-healing electrolyte with reduced conductivity, but stronger mechanical properties.[14] However, conventioanl electrolytes can be equipped with lithium salts or ionic liquids to adjust the conductivity and flexibility in order to gain sufficient conductivity. When used in 3D printing, the addition of fillers and hydrogen bonds to a thermoplastic polymer often lead to an increase of viscosity, whereas liquid fillers can reduce the viscosity in a polymer melt.[15] Thus, the addition of lithium salts to PEG polymers is a crucial parameter since the incorporation

of lithium ion into the crystalline parts of PEG can influence such mixtures in the direction of a more amorphous state.[16] Both, the quadruple hydrogen bonds and the lithium salt concentration in the PEG electrolyte are thus parameters useful for counterbalancing the viscosity of the polymer-melt at different temperatures.

We here report on the generation of solid electrolytes-materials, containing quadruple (UPy)-bonds and lithium-salts to adjust the printability of the so obtained electrolytes as shown in Figure 1. Based on a telechelic UPy-PEO/PPO-UPy-polymer, we find that there are three effects counterbalancing the rheological properties of the polymers: besides temperature, which can be used as a known tool to adjust melt-rheology, also the addition of lithium-salts in combination with the polymer's crystallinity exerts a major toolbox to affect printability of these electrolytes. To obtain knowledge about the interaction of lithium ions between the UPy end group and the polymer backbone FT-IR and DSC analyses were performed. Equipped with good conductivity, these materials represent a reasonable set of printable electrolytes, additionally displaying supramolecular (volume)-compensating effects.

2. Material Design and Components

The synthesis of the PEG-1500-UPy, JA-900-UPy, and JA-600-UPy polymers follows known procedures[13d], and is described in detail in the Supporting Information. A complete functionalization with the UPy-groups (UPy) was obtained by isocyanate addition to commercial PEO/PPO-NH$_2$-polymers, with a full NMR characterization (see Supporting Information).

For the formation of the polymer/Li-salt mixtures the PEG-1500-UPy, JA-900-UPy, and JA-600-UPy-polymers were dried in high vacuum for 3 h before use. Polymer electrolytes were prepared using a solution casting technique. Polymers and LiTFSI were dissolved in dry ACN and stirred for 4 h at room temperature. The molar ratio of EO/Li was set to 20:1, 10:1, and

2200088 (2 of 10)

Table 1. Prepared electrolyte mixtures of PEG-1500-UPy, JA-900-UPy, and JA-600-UPy with LiTFSI in different molar ratios EO/Li, respectively PO-EO/Li.

Entry	Polymer	M_w [Da]	a)Molar EO/Li b)Molar PO-EO/Li	ΔH_m [J g^{-1}]
1	**PEG-1500-UPy 1**	**2100**	–	17.4
2	PEG-1500-UPy 2	2100	40:1a)	18.9
3	PEG-1500-UPy 3	2100	20:1a)	6.0
4	PEG-1500-UPy 4	2100	15:1a)	–
5	PEG-1500-UPy 5	2100	10:1a)	–
6	PEG-1500-UPy 6	2100	8:1a)	–
7	PEG-1500-UPy 7	2100	6.7:1a)	–
8	PEG-1500-UPy 8	2100	5:1a)	–
9	**JA-900-UPy 9**	**1500**	–	30.2
10	JA-900-UPy 10	1500	20:1b)	18.8
11	JA-900-UPy 11	1500	10:1b)	–
12	JA-900-UPy 12	1500	5:1b)	–
13	**JA-600-UPy 13**	**1200**	–	42.7
14	JA-600-UPy 14	1200	20:1b)	5.9
15	JA-600-UPy 15	1200	10:1b)	–
16	JA-600-UPy 16	1200	5:1b)	–

a)Molar ration EO/Li; b)Molar ratio PO-EO/Li.

5:1 for each of the three polymers to study influences of the lithium-salt on the final rheological properties and thus on the 3D-printing abilities. The solution was cast in a PTFE mold and dried under vacuum at 70 °C for 48 h (**Table 1**).

3. 3D Printer

A grid with a 3D structure measuring with 6 × 6 mm square area was built accordingly to the created designs by means of the layer-by-layer deposition of the material. Two mutually perpendicular directions of the grid were used in alternating layers. Ten parallel polymer strands were printed in every layer and the gap between the strands is ca. 300 µm. For the finished the specimen, 4 layers were deposited. The 3D printer regenHU 3DDiscovery consists of a storage tank and a screw extruder, was used for printing of the polymer composites. We set a printing window by adjusting the printing temperature, pressure, screw speed, needle geometry, and movement speed of the printing head. The viscosity of the printable polymer blends was required from 200 to 2000 Pa s. After preheating to the required temperature, the samples were pushed into the screw extruder under high pressure (0.20 MPa) and then extruded through a metal needle with 330 µm inner diameter. The electrolytes were deposited on glass at room temperature. The movement speed of the printing head was 10 mm s^{-1}.[17] The finished 3D-printed samples were transparent and sensitive toward moisture.

4. FT-IR Analysis of Pure Polymers

The starting 2-ureido-4-pyrimidinone isocyanate (UPy-NCO), used for end group modification and the UPy-telechelic

polymers (PEG-1500-UPy 1, JA-900-UPy 9, JA-600-UPy 13) were analyzed by FT-IR spectroscopy to confirm their successful synthesis (**Figure 2**).[13d] The newly formed urea bonds show a band at 3336 cm^{-1} for the N-H stretch vibration.[18] No residual signal for the isocyanate (NCO) was observed for all modified polymers, which would be around 2275 cm^1.[19] Carbonyl groups from the new UPy endgroup at the polymer were visible at 1700 and 1665 cm^{-1}, with one of the main bands for the polymer backbone located at 1095 cm^{-1} representative for the C-O stretching vibration.[20] Additionally, NMR-spectroscopy confirms the chemical identities of the polymers (see Supporting Information).
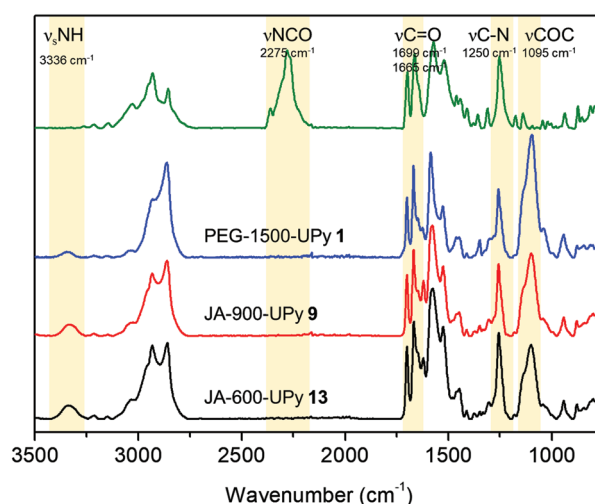

Figure 2. FT-IR spectra for the reaction products PEG-1500-UPy 1 (blue), JA-900-UPy 9 (red), and JA-600-UPy 13 (black) are shown without any residual isocyanate peak like for 2-ureido-4-pyrimidinone isocyanate (UPy-NCO, green).
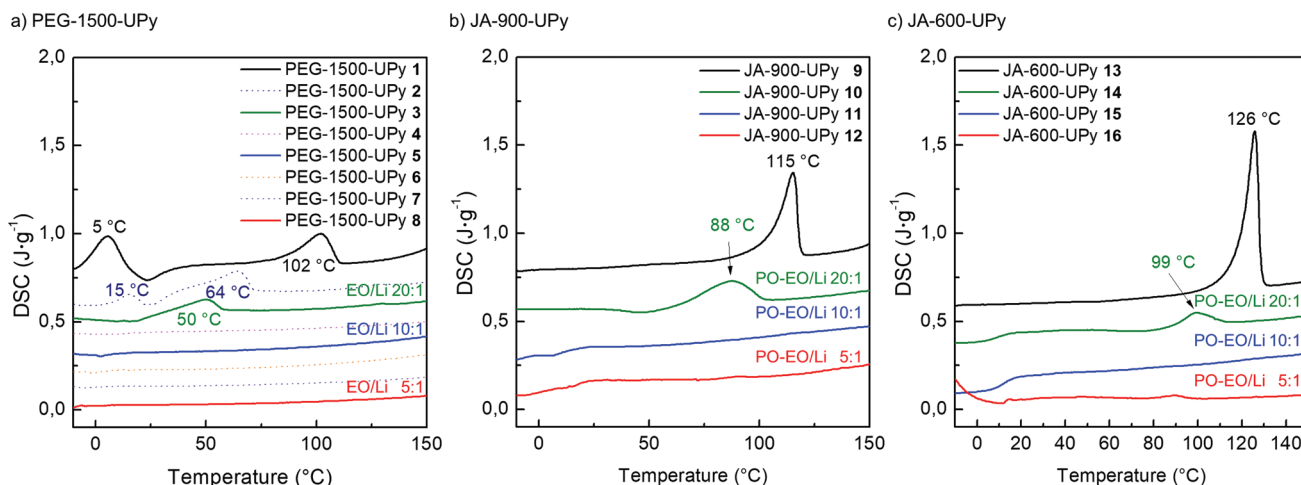
**ADVANCED
SCIENCE NEWS**

www.advancedsciencenews.com

**ADVANCED
MATERIALS
TECHNOLOGIES**

www.advmattechnol.de

Figure 3. Thermal behavior of a) PEG-1500-UPy 1–8, b) JA-900-UPy 9–12, and c) JA-600-UPy 13–16, as well as their mixtures with LiTFSI, in the ratio of EO/Li = 20:1, 10:1, and 5:1.

5. DSC of Electrolytes

In order to collect the first parameters for printability, we checked the thermal behavior of the mixtures. We thus conducted DSC measurements of polymer-UPy samples and electrolyte mixtures with different lithium concentrations in a temperature range of -10 to 150 °C with a heating rate of 10 K·min⁻¹ (**Figure 3**). In the case of pure PEG-1500-UPy 1 in Figure 3a, the melting peak at 5 and 102 °C is indicative for a phase separation between the EO-parts and the UPy-end groups, also demonstrated previously with SAXS by Brás et al.[21] These melting peaks shift for PEG-1500-UPy 2 and 3 closer together to 15 °C and 64 °C (2), as well as 50 °C (3). Samples with higher lithium concentrations, PEG-1500-UPy 5 (10:1) and PEG-1500-UPy 8 (5:1), suggested a purely amorphous material. For JA-900-UPy 9 in Figure 3b, the melting peak was located at 115 °C, whereas the melting peak for JA-900-UPy 10 (20:1) was found at 88 °C. With an increase in the amount of lithium-ions to JA-900-UPy 11 (10:1) and JA-900-UPy 12 (5:1), the glass transition temperatures changed to 15 °C. Pure JA-600-UPy 13 in Figure 3c showed a melting at the highest temperature of 126 °C, whereas the addition of LiTFSI caused significant changes, as the melting peak shifted toward lower temperatures. For JA-600-UPy 14 (20:1), melting was observed at 99 °C. A further increase of lithium salt in ratios of JA-600-UPy 15 (10:1) and JA-600-UPy 16 (5:1) resulted in an amorphous material with a glass transition at 13 °C. It can thus be concluded that the lithium ions did form coordinative interactions with the oxygen atoms of the PEG/PPG backbone, thus changing the crystalline-structure of the PEG, presumably hindering the formation of lamellar structures as indicated in literature for similar PEG/Li-ion based materials.[11,22]

6. Rheology of Electrolytes

3D-printability was investigated for the prepared polymer-UPy samples using melt-rheology measurements. Polymer-UPy samples were mixed with LiTFSI in molar ratios of EO/Li of 5:1, 10:1, and 20:1, dissolved in dry ACN, and stirred for 4 h at room temperature. The solvent was removed under vacuum and the mixtures were dried before rheology measurements. The printing window was determined as in our previous investigations,[17] being situated around a viscosity range of 200 – 2000 Pa·s. Before investigating polymer-UPy-Li mixtures, pure polymer-UPy samples were analyzed using melt rheology. The measurement results are shown in **Figure 4**a. A shear-thinning behavior can be seen in PEG-1500-UPy 1, not fitting into the desired printing window over a range of different shear rates. The viscosity of PEG-1500-UPy 1 dropped from 10^3 to 10^1 Pa·s for the temperatures range of 110 to 130 °C, clearly indicative of the thermal effect on the UPy-quadruple hydrogen bonds shifting the supramolecular equilibrium of the H-bonds to the open/non-associated side. However, this large shear thinning behavior of the material makes the polymer unsuitable for FDM printing.

We then investigated the mixtures of PEG-1500-UPy 3,5,8 in molar ratios of EO/Li adjusted to 20:1, 10:1, and 5:1, respectively. After the addition of the lithium ions, the viscosity is decreased for low lithium concentrations and later increased for high lithium concentrations. We consider that there are two effects, counterbalancing each other: on the one hand, the lithium ions interact with the EO repeating units and form coordination bonds, leading to a potential increase in viscosity. On the other hand, the lithium ions hinder the packing of PEG molecules and thus lead to a decrease in crystallinity that results in a reduced viscosity in the observed temperature region. Additionally, we expected a gradual weakening of the quadruple hydrogen bonds by the subsequent addition of lithium-ions. As a gradual formation of plateau values for the viscosity can be observed for an increasing lithium concentration, we interpret this as the interaction between the lithium ions and the hydrogen bonds of the polymer backbone/end groups. As shown in Figure 4a, with a molar ratio of 20:1, the shear-thinning behavior is not changed considerably in terms of viscosity values for temperatures 30 to 50 °C, although the shift to higher viscosity at a higher shear rate of 10 s¹ confers the effect

**ADVANCED
SCIENCE NEWS**
www.advancedsciencenews.com

**ADVANCED
MATERIALS
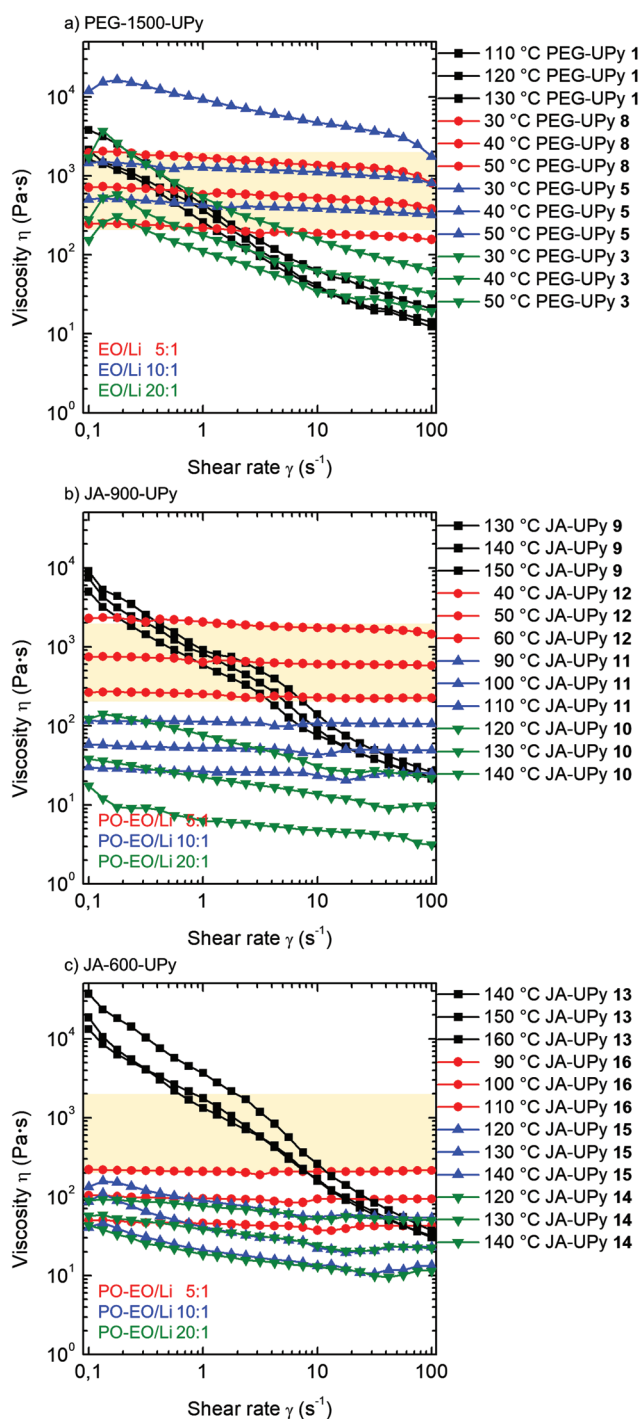TECHNOLOGIES**
www.advmattechnol.de

Figure 4. Rheology measurements of viscosity-shear rate-temperature dependence for a) PEG-1500-UPy 1,3,5,8, b) JA-900-UPy 9–12, and c) JA-600-UPy 13–16 c) to test for the printing window of 200 to 2000 Pa s.

of mixing with the lithium ions. A further increase to a molar ratio of 10:1, as shown in Figure 4a, shifting the viscosity from 10^4 to 10^2 Pa·s in the range of 30 to 50 °C. However, the viscosity values now fit into the printing window perfectly and the generated plateau displays a shear-independent viscosity over a high shear rate values that is suitable for 3D-printing. With

a molar ratio EO/Li of 5:1 this resulted in a viscosity range of 10^3–10^2 Pa·s at temperatures 30 to 50 °C, completely fitting into the printing window and thus being suitable for 3D-printing.

For JA-900-UPy **9**, a steep shear thinning behavior can be seen, not fitting into the printing window (Figure 4b). As the concentration of lithium ions increases in the matrix, the viscosity forms a plateau region ≈10^3–10^2 Pa s for molar ratios **10** ((P)EO/Li = 20:1), **11** (10:1), and **12** (5:1), respectively at high temperatures of 90–140 °C, except for the composition **12** (5:1) at 60 °C. The viscosity values now fit into the printing window for temperatures of 130–140 °C or 50 °C and are thus suitable for 3D-printing.

JA-600-UPy **13** and mixtures of JA-600-UPy-Li in molar ratios of EO/Li **14** (20:1), **15** (10:1), and **16** (5:1) were generated and the measured results are shown in Figure 4c. A steep shear thinning behavior can be seen for JA-600-UPy **1** from viscosity values 10^4 –10^2 Pa·s at temperatures 140 to 160 °C that clearly are not fitting into the printing window. With a gradual increase in lithium ions concentration, the viscosity decreased, again assigned to the hindered packing of PEO molecules, concomitant to a decrease in crystallinity of the sample. Large amounts of lithium ions present within the polymer matrix improve the mechanical strength of the matrix, resulting in increasing viscosity values. Among the tested molar ratios of EO/Li, **16** (5:1) displayed viscosity values of 10^3 –10^2 Pa·s at 120 °C.

Summarizing the complex results for viscosity-shear rate-temperature dependent measurements, it can be concluded that for FDM a high content of LiTFSI in PEG-1500-UPy, JA-900-UPy, and JA-600-UPy based electrolyte mixtures are required to achieve printability via the 3D-printed present in our setup. Furthermore, we observe a complex interplay of lithium-ions on the EO-units, their crystallinity, as well as on the dynamics of the quadruple-hydrogen bonds. Overall, it was satisfactory to see that addition of the LiTFSI-salts commonly used in the electrolyte systems is useful to achieve printability of the PEO-based supramolecular system.

7. Broadband Dielectric Spectroscopy

Conductivity measurements of the polymer/LiTFSI-composites were carried out using a Broadband Dielectric spectrometer (BDS) "Alpha analyzer" (Novocontrol). Two different sample cells were used depending on the sample texture. The sample cell for the soft gel polymer electrolytes consists of two brass electrodes having a sample space of 20 mm diameter and a thickness of 0.25 mm. Gels were carefully filled into the space between the electrodes inside the sample holder, avoiding air bubble formation. The polymer electrolyte gel with larger viscosity was solvent cast into a self-standing film of 20 mm in diameter and 0.4 mm in thickness. Subsequently, the film was sandwiched between two brass electrodes for the dielectric measurement. As the polymer electrolytes are hygroscopic in nature due to the presence of LiTFSI in the mixture, the measurements were performed inside a cryostat with a constant flow of dry nitrogen gas during the measurements. BDS measurements were performed in a frequency range of 1 Hz up to 10^6 Hz. Values of the DC-conductivity were extracted from the DC plateau of the log σ vs log frequency plots (see

**ADVANCED
SCIENCE NEWS**
www.advancedsciencenews.com

**ADVANCED
MATERIALS
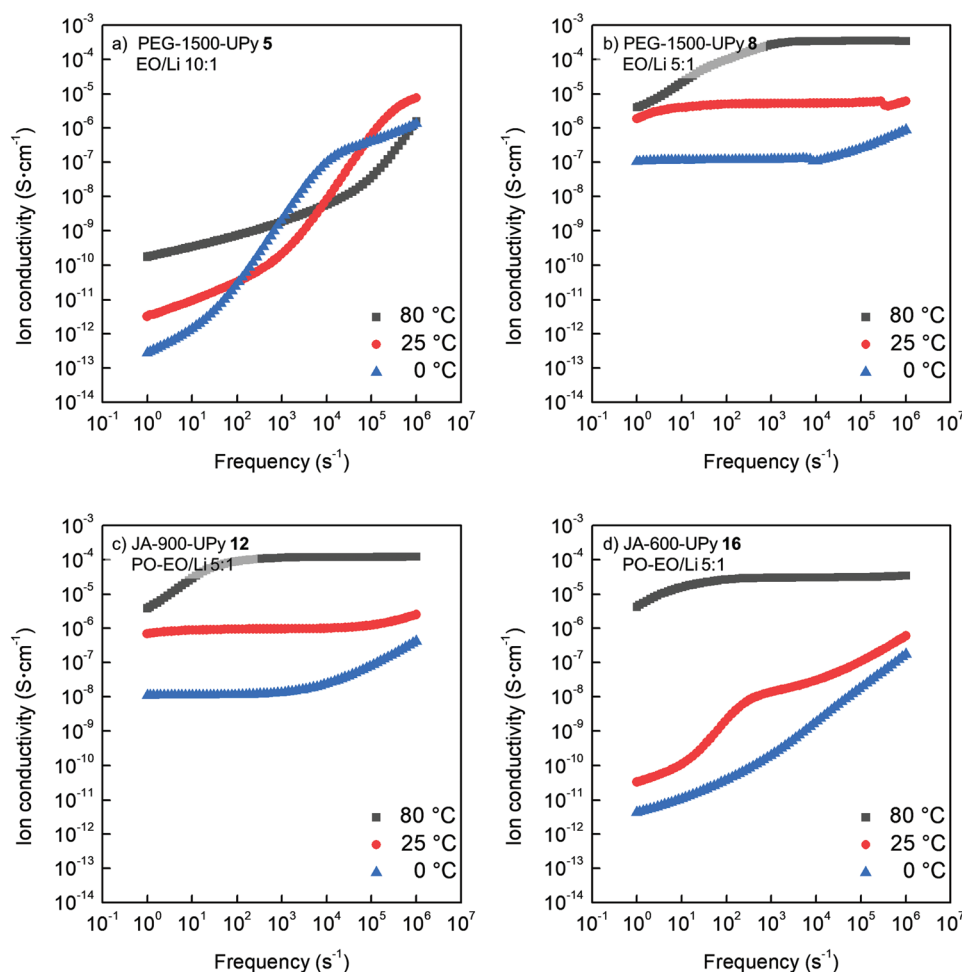TECHNOLOGIES**
www.advmattechnol.de

Figure 5. Broadband Dielectric Spectroscopy measurements of frequency dependent ionic conductivity at three different temperatures 80, 25, and 0 °C for a) PEG-1500-UPy 5 (10:1), b) PEG-1500-UPy 8 (5:1), c) JA-900-UPy 12 (5:1), and d) JA-600-UPy 16 (5:1).

Table S3, Supporting Information), reaching conductivites of up to 10^{-4} Scm^{-1} at 80 °C for the polymer/LiTFSi-mixture **8**, **12**, and **16**, containing a ratio [EO]/[Li] = 5/1 **Figure 5**.

8. FT-IR: Interaction of LiTFSI between PEG Backbone and UPy End Group

For a more detailed understanding of the Li/PEO-UPy interactions, we conducted FT-IR-spectra to discriminate between the different effects of lithium ion intercalation and its effect on the UPy-quadruple hydrogen bonds. The FT-IR spectra parts of PEG-1500-UPy/LiTFSI polymer electrolytes of different concentrations and PEG-1500-NH$_2$/LiTFSI are provided in the Supporting Information (Figure S7, Supporting Information). The analysis of characteristic peaks for the interaction of LiTFSI with a polymer was accomplished [23] (**Figure 6**). Peaks from the pure compounds PEG-1500-UPy **1** and PEG-1500-NH$_2$ shifted or changed intensity, indicating the interaction between both and so the dissolution of lithium in the PEG phase. Signals, which are not shifting, should therefore not be involved in the interaction of lithium salt with either UPy end group or PEG backbone.

The increase of LiTFSI concentration led to an increase of the absorbance related to it. Significant changes were observed for the CF$_3$ asymmetric vibration (v_aCF$_3$ = 1189 cm^{-1}) and the SNS asymmetric vibration (v_aSNS = 1060 cm^{-1}) (Figure 6a,d). Accordingly, the absorbance of PEG related peaks decreased, in detail the CH$_2$ peaks (vCH$_2$ = 2931 cm^{-1}, 2862 cm^{-1}), the carbonyl signals (vC = O = 1700 cm^{-1}, 1667 cm^{-1}) and the backbone ether signal (vCOC = 1097 cm^{-1}) (Figure S7, Supporting Information). For the end group UPy, the urea group (vNH = 3336 cm^{-1}) decreased and strongly shifted with increasing lithium salt content to 3411 cm^{-1} (Figure 6c). The peak of CH$_2$ of the PEG backbone (2862 cm^{-1}) is shifting with the increasing salt concentration to higher values.

The results were analyzed for the goal of ion interaction between lithium salt and PEG backbone or UPy end group, respectively. The different interactions play a major role in polymer electrolytes regarding physical and electrochemical properties.[6a,14a,24] Starting with two peaks based on LiTFSI in the mixtures, the vCF$_3$ (1189 cm^{-1}) continuously increases in intensity for higher salt contents, together with a peak shift to 1182 cm^{-1} (Figure S7, Supporting Information,and 6a).[23a] PEG-1500-UPy and PEG-1500-NH$_2$ are very similar in this IR
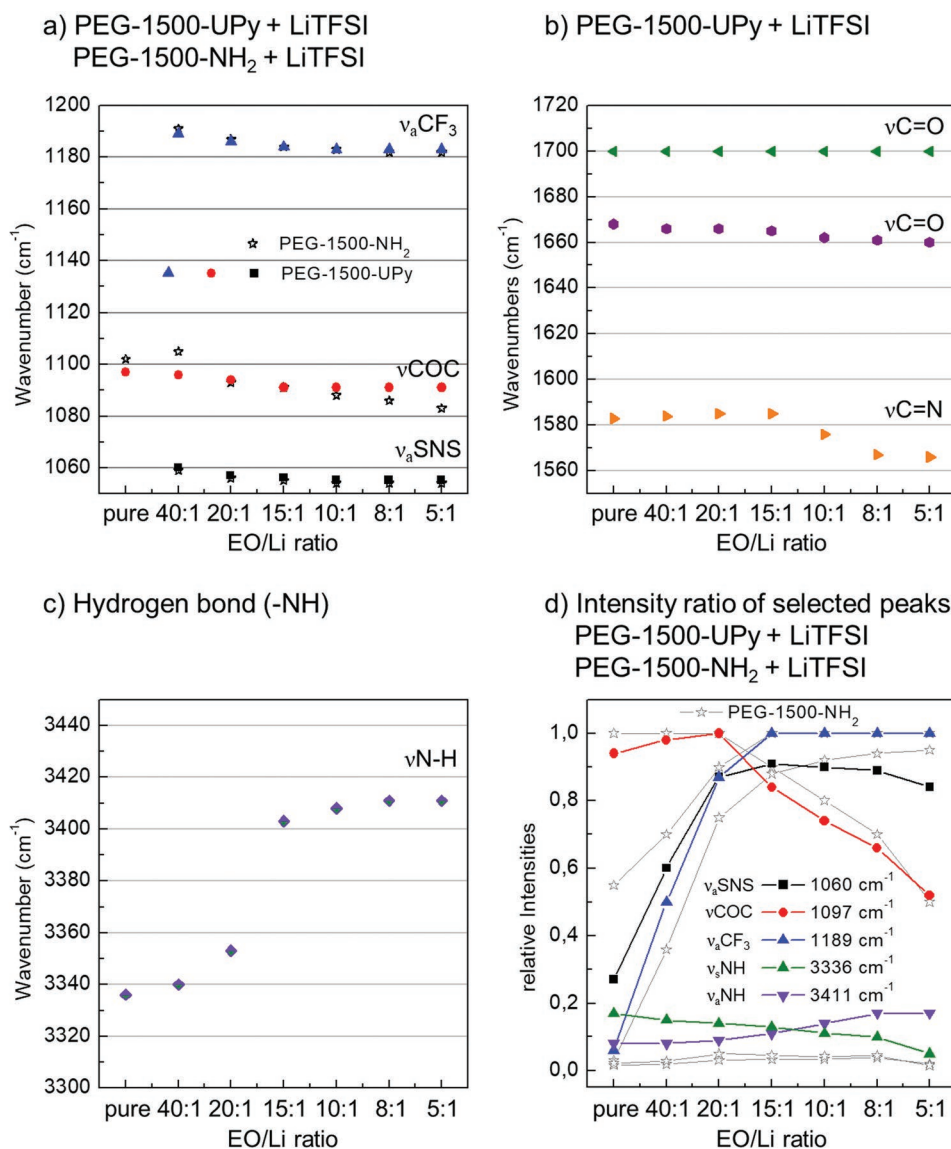
Figure 6. Detailed FT-IR analysis of PEG-1500-UPy and PEG-1500-NH$_2$, as well as its mixtures with increasing LiTFSI content 2–8. Increasing lithium salt content results in peak shifts of a) the polymer backbone, b) the UPy end group, c) the hydrogen bonds, and d) intensity variation due to different interactions of lithium ions with UPy and PEG.

band. This shift was rarely discussed in literature before and an explanation could be related to the strong electron-negativity of fluorine or delocalized negative charge, as well as conformational changes of TFSI, phase separation or Li-F coordination.[25] The IR band νSNS (1060 cm^{-1}) is also shifting to a lower wavelength with increasing concentration (1054 cm^{-1}) which is in agreement with other research (Figure 6a).[23a,d] The intensity increase is similar to CF$_3$ band (Figure S7, Supporting Information). The behavior of PEG-1500-UPy and PEG-1500-NH$_2$ is the same for this band. Switching over to the polymer backbone of PEG, the important band νCOC at 1097 cm^{-1} is related to the crystalline structure of PEG being strong in intensity below the melting point,[26] and shifts to a lower wavelength of 1087 cm^{-1} (Figure 6a). The band shift for PEG-1500-NH$_2$ is much stronger from 1102 cm^{-1} to 1083 cm^{-1} (Figure 6a). The decrease of intensity is more significant at lower salt concentrations

for PEG-1500-UPy compared to PEG-1500-NH$_2$ (Figure S7, Supporting Information), which is related to their different crystallinities. At very low LiTFSI concentration, the crystalline structure stays intact and is not disturbed by the lithium ions. With increasing lithium concentration, the intensity decreases. Other effects influencing the decrease of intensity could be the dilution of the ether group by the salt concentration or the change of COC conformation. The lithium salt can form crown-ether-like coordination structures with the PEG backbone.

The interaction of LiTFSI with the UPy end group undergoes a different mechanism, due to the dipolar and hydrogen-bonding character of the UPy group. We propose that the urea part of the UPy end group binds with the lithium ion and forms a lithium-metal complex via the oxygen of the carbonyl group due to stronger electronegativity. The change in carbonyl band maxima is not measurable for 1700 cm^{-1}, but the carbonyl band

**ADVANCED
SCIENCE NEWS**

www.advancedsciencenews.com

**ADVANCED
MATERIALS
TECHNOLOGIES**

www.advmattechnol.de

1668 cm^{-1} shifts slightly to 1660 cm^{-1} (Figure 6b).[23b] In contrast a larger shift is observed for vibrations containing nitrogen atoms like C=N (1585 cm^{-1}) shifting to 1566 cm^{-1} (Figure 6b). The hydrogen bonding (N–H$\cdots$O) between the NH group and carbonyl C=O results in a specific peak at 3336 cm^{1}. When adding LiTFSI, the NH peak gets strongly changed, as the NH band slowly blue-shifts at low lithium concentrations, later starts to form a new peak at 3411 cm^{-1} (Figure 6c).[23c] This strong shift indicates breaking of hydrogen bonds within the UPy end group. The change from symmetric NH vibration to the asymmetric NH vibration with increasing lithium content corresponds to more free NH groups.[27] The results suggest that the hydrogen bonds are weakened or broken due to lithium interaction with UPy end groups.

Based on normalized FTIR spectra, a comparison between the intensity ratio of νCF$_3$, νCOC, νSNS can be done. Figure 6d just gives the dominant band between these three important bands. For low salt concentrations (up to PEG-1500-UPy 3), the band νCOC corresponding to the PEG backbone and related to its crystallinity was the strongest band for both, PEG-1500-UPy and PEG-1500-NH$_2$. Please note, that the absolute values for the crystalline PEG-1500-NH$_2$ are much larger. Between PEG-1500-UPy 3 and 4, the dominance in the FTIR spectra changes to the νCF$_3$ band of the lithium salt, whereafter the increase of the LiTFSI bands is much stronger than the reduction of νCOC band intensity. Such a shift after PEG-1500-UPy 3 is also observed for the change from symmetric NH vibration to the asymmetric NH vibration (Figure 6c). At a concentration of LiTFSI higher than EO/Li of 20:1, the hydrogen bonds of UPy end groups therefore can be assumed to dissociate, indicated

by a continuous movement of the NH band toward 3411 cm^{-1} (Figure S7, Supporting Information)—an effect clearly assigned to the UPy end groups.

9. Fused Deposition Modeling

Selected polymer electrolytes were extruded with an FDM printer directly onto a glass slide. JA-900-UPy 12 (5:1) was printed at $140\,°C$ and the freshly printed grid was photographed (**Figure 7**). After printing, the structural stability was checked by observation of printed structures at room temperature. When the samples were located under normal air, a shape loss took place due to water absorption of the electrolyte. A different shape with the same material is based on a dense grid structure in Figure 7c proving the flexibility in shapes. In Figure 7d, the printed result for PEG-1500-UPy 8 (5:1) is shown in a lamella style, but due to the low glass transition temperature of the mixture, the material spreads after extrusion. The printing temperature for the PEG mixture was set to $90\,°C$. The sample most suited for an easy self-healing test was JA-900-UPy 12 (Figure 7e) displaying amorphous, little elastic properties; it was prepared in a tablet-specimen as a simple preparation method and easy to cut. The sample did partly reconnect after the cut, when stored in a glovebox for 4 h at room temperature. Mixtures with low lithium salt content (ratio 20:1) were still too crystalline and thus not suitable for tests at room temperature. The samples with PEG-1500-UPy 5 and 8 were to sticky and viscous not able to form a clean tablet-specimen for testing.
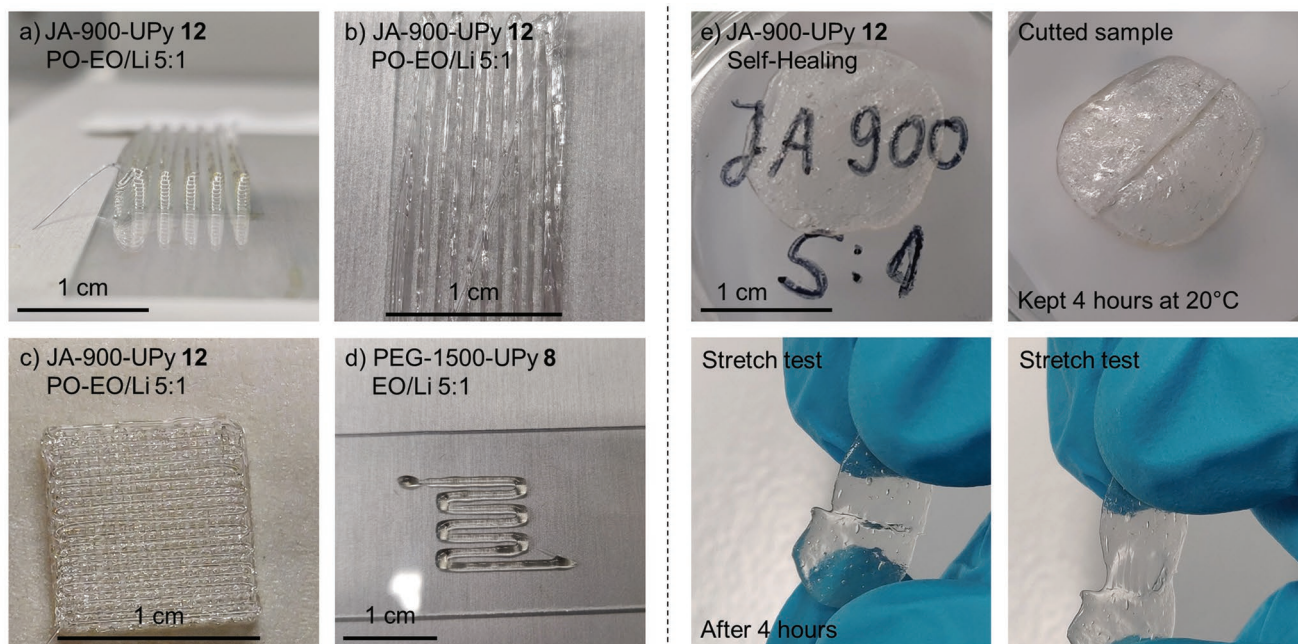

Figure 7. Showcase of 3D-printed JA-900-UPy 12 (5:1) in different shapes like a freestanding lamella structure (a, b, 10 mm × 20 mm) and a grid (c, 10 mm × 10 mm). The freshly printed structures a–c showed uniform strands and gaps, stable after 3D printing under an inert atmosphere. The PEG-1500-UPy 8 (5:1) printed lamellay were not stable after extrusion and did spread on the glass slide. For JA-900-UPy 12, an easy self-healing test was performed with a disc-shaped specimen being cut in half and reconnected. e) Already after 4 h at room temperature a reconnection between the two halves was observed.

10. Conclusions

We here report the 3D printing of a supramolecular and conductive polymer, able to be manufactured via 3D printing processes. Affixed quadruple-hydrogen bonds (UPy-groups) additionally embed dynamic properties into the electrolyte, which potentially allows self-restorative properties, dynamically compensating for volume changes. The here generated solid electrolytes-materials, contain quadruple (UPy)-bonds and lithium-salts to adjust the conductivity and printability of the electrolytes. We have synthesized different telechelic UPy-PEO/PPO-UPy-polymers, differing in their rheological profile, which allows a further adjustment of their printability by FDM-processes. We find that there are three effects counterbalancing the rheological properties of the polymers: besides temperatures, which can be used as a known tool to adjust melt-rheology, also the addition of lithium salts in junction with the polymer's crystallinity exerts a major toolbox to affect the printability of these electrolytes. Using specific compositions between the Li/EO-ratios from EO/Li 20:1, 10:1, and 5:1 we could adjust the rheological profile to the printability window. The performed FT-IR-investigations clearly indicate a weakening of the UPy-bonds by the added lithium ions, in addition to a reduction of the crystallinity of the PEO units, further changing the rheological profile. Equipped with good conductivity, these materials represent a reasonable set of printable electrolytes, additionally displaying self-healing, (volume)-compensating effects.

A careful mechanical design, in addition to rheological effects observed for different additives to the electrolyte is investigated and adjusted, in order to achieve printability via an extrusion process to generate a conductive electrode material.

Supporting Information

Supporting Information is available from the Wiley Online Library or from the author.

Conflict of Interest

The authors declare no conflict of interest.

Data Availability Statement

The data that support the findings of this study are available from the corresponding author upon reasonable request.

[1] D. Chen, D. Wang, Y. Yang, Q. Huang, S. Zhu, Z. Zheng, *Adv. Energy Mater.* **2017**, *7*, 1700890.

[2] G. Hou, B. Cheng, Y. Cao, M. Yao, B. Li, C. Zhang, Q. Weng, X. Wang, Y. Bando, D. Golberg, F. Yuan, *Nano Energy* **2016**, *24*, 111.

[3] A. Marinow, H. Rupp, W. H. Binder, *Chemie in unserer Zeit* **2021**, *55*, 422.

[4] C. Wang, H. Wu, Z. Chen, M. T. Mcdowell, Y. Cui, Z. Bao, *Nat. Chem.* **2013**, *5*, 1042.

[5] a) A. Campanella, D. Döhler, W. H. Binder, *Macromol. Rapid Commun.* **2018**; b) T. Aida, E. W. Meijer, *Isr. J. Chem.* **2020**, *60*, 33.

[6] a) G. Zhang, Y. Yang, Y. Chen, J. Huang, T. Zhang, H. Zeng, C. Wang, G. Liu, Y. Deng, *Small* **2018**, *14*, 1801189; b) J. Yang, L. Zhang, T. Zhang, X. Wang, Y. Gao, Q. Fang, *Electrochem. Commun.* **2018**, *87*, 22.

[7] a) A. Maurel, M. Armand, S. Grugeon, B. Fleutot, C. Davoisne, H. Tortajada, M. Courty, S. Panier, L. Dupont, *J. Electrochem. Soc.* **2020**, *167*, 070536; b) M. Cheng, M. Cheng, R. Deivanayagam, R. Shahbazian-Yassar, *Batteries Supercaps* **2020**, *3*, 130; c) A.-N. Chen, C. Qu, Y. Shi, F. Shi, *Front. Energy Res.* **2020**, *8*, 226; d) T. S. Arthur, D. J. Bates, N. Cirigliano, D. C. Johnson, P. Malati, J. M. Mosby, E. Perre, M. T. Rawls, A. L. Prieto, B. Dunn, *MRS Bull.* **2011**, *36*, 523.

[8] a) B. Trembacki, E. Duoss, G. Oxberry, M. Stadermann, J. Murthy, *J. Electrochem. Soc* **2019**, *166*, A923; b) H. Ragones, S. Menkin, Y. Kamir, A. Gladkikh, T. Mukra, G. Kosa, D. Golodnitsky, *Sustain. Energy Fuels* **2018**, *2*, 1542.

[9] a) C. Reyes, R. Somogyi, S. Niu, M. A. Cruz, F. Yang, M. J. Catenacci, C. P. Rhodes, B. J. Wiley, *ACS Appl. Energy Mater.* **2018**, *1*, 5268; b) T.-S. Wei, B. Y. Ahn, J. Grotto, J. A. Lewis, *Adv. Mater.* **2018**, *30*, 1703027.

[10] A. Maurel, M. Courty, B. Fleutot, H. Tortajada, K. Prashantha, M. Armand, S. Grugeon, S. Panier, L. Dupont, *Chem. Mater.* **2018**, *30*, 7484.

[11] A. R. Polu, H.-W. Rhee, *Sci. Adv. Mater.* **2016**, *8*, 931.

[12] a) D. Lin, W. Liu, Y. Liu, H. R. Lee, P.-C. Hsu, K. Liu, Y. Cui, *Nano Lett.*. **2016**, *16*, 459; b) Y. E. Wang, W. D. Richards, L. J. Miara, J. C. Kim, G. Ceder, presented at *ECS Meeting Abstracts* **2016**, p. 456; c) Y. Zhao, Y. Zhang, H. Sun, X. Dong, J. Cao, L. Wang, Y. Xu, J. Ren, Y. Hwang, I. H. Son, X. Huang, Y. Wang, H. Peng, *Angew. Chem., Int. Ed.* **2016**, *55*, 14384.

[13] a) T. F. A. De Greef, M. M. J. Smulders, M. Wolffs, A. P. H. J. Schenning, R. P. Sijbesma, E. W. Meijer, *Chem. Rev.* **2009**, *109*, 5687; b) J. H. K. K. Hirschberg, A. Ramzi, R. P. Sijbesma, E. W. Meijer, *Macromolecules* **2003**, *36*, 1429; c) S. H. M. Söntjens, R. P. Sijbesma, M. H. P. Van Genderen, E. W. Meijer, *J. Am. Chem. Soc.* **2000**, *122*, 7487; d) B. J. B. Folmer, R. P. Sijbesma, R. M. Versteegen, J. A. J. Van Der Rijt, E. W. Meijer, *Adv. Mater.* **2000**, *12*, 874; e) R. P. Sijbesma, F. H. Beijer, L. Brunsveld, B. J. B. Folmer, J. H. K. K. Hirschberg, R. F. M. Lange, J. K. L. Lowe, E. W. Meijer, *Science* **1997**, *278*, 1601; f) F. H. Beijer, R. P. Sijbesma, H. Kooijman, A. L. Spek, E. W. Meijer, *J. Am. Chem. Soc.* **1998**, *120*, 6761.

[14] a) B. Zhou, D. He, J. Hu, Y. Ye, H. Peng, X. Zhou, X. Xie, Z. Xue, *J. Mater. Chem. A* **2018**, *6*, 11725; b) Y. H. Jo, B. Zhou, K. Jiang, S. Li,

C. Zuo, H. Gan, D. He, X. Zhou, Z. Xue, *Polym. Chem.* **2019**, *10*, 6561.

[15] H. Rupp, W. H. Binder, *Front. Chem.* **2021**, *9*, 771974.

[16] a) D. E. Fenton, J. M. Parker, P. V. Wright, *Polymer* **1973**, *14*, 589; b) M. B. Armand, J. M. Chabagno, M. J. Duclot, *Fast Ion Transp. Solids: Electrodes Electrolytes, Proc. Int. Conf.* (Eds: P. Vashishta, J. N. Mundy, G. K. Shenoy), **1979**, pp. 132–136; c) F. M. Gray, *Polymer electrolytes*, Royal Society of Chemistry, **1997**; d) C. Sequeira, D. Santos, *Polymer electrolytes: fundamentals and applications*, Elsevier, **2010**.

[17] a) H. Rupp, D. Döhler, P. Hilgeroth, N. Mahmood, M. Beiner, W. H. Binder, *Macromol. Rapid Commun.* **2019**, *40*, 1900467; b) H. Rupp, W. H. Binder, *Adv. Mater. Technol.* **2020**, *5*, 2000509; c) H. Rupp, W. H. Binder, *Macromol. Rapid Commun.* **2021**, *42*, 2000450.

[18] S. Zhang, Z. Ren, S. He, Y. Zhu, C. Zhu, *Spectrochim. Acta A Mol. Biomol. Spectrosc.* **2007**, *66*, 188.

[19] A. Friebe, H. W. Siesler, *Vib. Spectrosc.* **2007**, *43*, 217.

[20] a) D. J. M. Van Beek, A. J. H. Spiering, G. W. M. Peters, K. Te Nijenhuis, R. P. Sijbesma, *Macromolecules* **2007**, *40*, 8464; b) S. Bobade, Y. Wang, J. Mays, D. Baskaran, *Macromolecules* **2014**, *47*, 5040.

[21] A. Brás, A. Arizaga, U. Agirre, M. Dorau, J. Houston, A. Radulescu, M. Kruteva, W. Pyckhout-Hintzen, A. M. Schmidt, *Polymers* **2021**, *13*, 2235.

[22] a) G. S. Macglashan, Y. G. Andreev, P. G. Bruce, *Nature* **1999**, *398*, 792; b) D. G. Kwabi, N. Ortiz-Vitoriano, S. A. Freunberger, Y. Chen, N. Imanishi, P. G. Bruce, Y. Shao-Horn, *MRS Bull.* **2014**, *39*, 443; c) M. Ati, W. T. Walker, K. Djellab, M. Armand, N. Recham, J.-M. Tarascon, *Electrochem. solid-state lett.* **2010**, *13*, A150; d) D. Zhou, D. Shanmukaraj, A. Tkacheva, M. Armand, G. Wang, *Chem* **2019**, *5*, 2326.

[23] a) K. Kim, L. Kuhn, I. V. Alabugin, D. T. Hallinan Jr., *Front. Energy Res.* **2020**, *8*, 240; b) H. Liang, H. Li, Z. Wang, F. Wu, L. Chen, X. Huang, *J. Phys. Chem* **2001**, *105*, 9966; c) R. Chen, F. Wu, Li, B. Xu, X. Qiu, S. Chen, *J. Phys. Chem* **2007**, *111*, 5184; d) W. Kam, C.-W. Liew, J. Y. Lim, S. Ramesh, *Ionics* **2014**, *20*, 665.

[24] a) B. Zhou, Y. H. Jo, R. Wang, D. He, X. Zhou, X. Xie, Z. Xue, *J. Mater. Chem. A* **2019**, *7*, 10354; b) X. Chen, C. E. Zawaski, G. A. Spiering, B. Liu, C. M. Orsino, R. B. Moore, C. B. Williams, T. E. Long, *ACS Appl. Mater.* **2020**, *12*, 32006.

[25] a) M. Herstedt, M. Smirnov, P. Johansson, M. Chami, J. Grondin, L. Servant, J. C. Lassègues, *J. Raman Spectrosc.* **2005**, *36*, 762; b) R. Arnaud, D. Benrabah, J-Y. Sanchez, *J. Phys. Chem* **1996**, *100*, 10882.

[26] a) A. Bakker, *Polymer* **1995**, *36*, 4371; b) A. Bakker, J. Lindgren, K. Hermansson, *Polymer* **1996**, *37*, 1871; c) H. Zhang, J. Wang, *Spectrochim. Acta A Mol. Biomol. Spectrosc* **2009**, *71*, 1927.

[27] R. A. Nyquist, *Interpreting infrared, Raman, and nuclear magnetic resonance spectra*, Academic Press, **2001**.